



Study of optical and laser damage threshold in EDTA and DTPA-doped DAST single crystals

M. Manivannan¹ · S. A. Martin Britto Dhas¹ · M. Balakrishnan² · M. Jose¹

Received: 19 March 2018 / Accepted: 26 July 2018 / Published online: 2 August 2018
© Springer-Verlag GmbH Germany, part of Springer Nature 2018

Abstract

We report the influence of EDTA and DTPA on the optical and laser damage thresholds of industrially relevant 4-dimethylamino-*N*-methyl stilbazolium tosylate (DAST) single crystals. Single crystal X-ray diffraction and powder X-ray diffraction studies substantiate that they crystallize in monoclinic system. The dopants facilitate tuning of the refractive indices and their optical conductivity. The laser damage threshold values of EDTA and DTPA-doped DAST crystals were found to be 1.5 and 1.6 times higher than the pure DAST crystal. The voltage-dependant photoconducting studies performed at ambient conditions shows negative photoconducting nature for pure and EDTA-doped DAST crystals while positive photoconducting nature is noticed for DTPA-doped crystal. The etching studies demonstrate the quality of the doped DAST crystals is better than the pure one.

1 Introduction

During the twenty-first century, a lot of research interest is devoted to the investigation of nonlinear optical materials due to their attractive physical properties such as large thermal stability, optical transparency, optical and mechanical stabilities leading to the realization of number of applications in industry [1–4]. The efficiency of NLO materials mainly depends on their ability for withstanding high power lasers sources [5]. In addition, the materials with large second order nonlinearities (SHG), high thermal stability, better mechanical properties and larger transparency band width are very essential to realize number of applications. Therefore, the synthesis of novel materials with enhanced NLO properties is of significant research interest. Among the non linear optical materials, inorganic materials like GaAs, InP and LiNbO₃ are widely utilized in number of optoelectronic devices because of their high mechanical strength, high melting point and chemical inertness, however, their optical non-linearity is very low due to the lack of delocalized π -electron in these materials [6, 7]. Therefore, alternatively, there is

a great demand for organic crystals due to their high laser damage threshold, large optical nonlinearity, high electronic susceptibilities, larger photochemical stabilities, large packing densities, higher molecular polarizability, π -conjugated electron and flexibility [4, 8]. Developing and designing the organic molecular crystals with suitable acceptor and donor has turned into a big deal of consideration. For the last few years, much effort was taken towards the development of novel organic materials for THz generators and detectors with the suitable strengths such as high signal to noise ratio, high peak electric field and broad band width [9].

THz radiation is generated by several methods, such as optical rectification, difference frequency generation, photoconductive switching, free electron laser and electro optic sampling [10, 11]. Organic ionic crystal of 4-dimethylamino-*N*-methyl stilbazolium tosylate (DAST) is a potential material with higher nonlinear optical susceptibility, refractive index, electro optical (EO) coefficients, figure of merit, shorter response time and low dielectric constant among the currently existing organic crystals [12, 13]. The large NLO susceptibility of DAST crystal has fascinated a conceivable interest owing to the potential uses in high frequency electro optic modulation, frequency conversion, telecommunication, data storage, optical signal processing, molecular electronics, laser remote sensing, integrated photonics, and Terahertz (THz) generation and detection [14]. Bulk size and good quality crystals are the prerequisite factors for designing devices for reliable applications but the growth of bulk size

✉ M. Jose
mjosh1231@gmail.com; jose@shcpt.edu

¹ Department of Physics, Sacred Heart College (Autonomous), Tirupattur, Tamilnadu, India

² Department of Physics, Government Arts College, Thiruvannamalai, Tamilnadu, India

DAST crystal without mis-orientation, imperfect surface, in-homogeneity and non-flatness state is quite a difficult task [12]. To overcome these difficulties, several research groups are involved in optimizing the growth techniques, which rendered a special focus on DAST crystal for various applications [15].

Ethylene diamine tetraacetic acid (EDTA) and Diethylene triamine pentaacetic acid (DTPA) are found to be excellent additives in the growth process due to their trace metal in the solution and controlling the formation of the clusters and nuclei by absorbing the metallic ion present in the materials. Moreover, EDTA forms ionized complexes with the metal ions impurities and reduce the chemical reactions. Similarly, the five acetate moieties of DTPA create a strong bond with the material and become more stable compared to EDTA [16, 17]. A very small amount of additives may significantly reduce the multi-nucleation and increase the quality of the single crystal [18]. Further, these additives increase the metastable zone width, growth rate, and reduce the secondary nucleations, which would enhance the quality of the crystals [16, 19].

This article demonstrates the growth of bulk size DAST crystal by the influence of additives (EDTA and DTPA). The crystals were successfully grown with good quality and bulk size by slow solvent evaporation technique at ambient temperature. The structural and crystal parameters of good quality grown crystals were recognized by single crystal (SXRD) and powder X-ray diffraction (PXRD) studies. The energy band gap and optical parameters were determined using UV–visible spectroscopy. Linear refractive indices of pure, DTPA and EDTA-doped DAST crystals were found to be 2.43, 2.51 and 2.60 at 800 nm. Laser damage threshold of EDTA and DTPA-doped DAST crystals showed a better performance than pure DAST crystals. The impact of charge carrier and life time of photons during light irradiation of pure and additives added DAST crystals has been enumerated using photoconductivity analysis. The presence of crystal defects and dislocations are examined by solvent etching technique and it reveals fewer dislocations in doped crystals.

2 Experimental details

2.1 Material preparation and crystal growth

DAST raw material was prepared by condensation of 4-picoline, methyl toluenesulphonate and 4-*N,N*-dimethylamino benzaldehyde with piperidine as catalyst according to the literature [20]. The final red precipitate was dried at 120 °C to get rid of chemisorbed water molecules and the purity was enhanced by repeated recrystallization process. The saturated DAST solution was prepared using methanol at ambient temperature and positioned for the growth. Simultaneously, required amount of additives EDTA and DTPA (0.001, 0.002 and 0.01 M) were added individually and stirred well with the DAST solution. The saturated solutions were filtered and covered with a polyethylene sheet to control the rate of solvent evaporation and kept away from mechanical shake. After the period of over 23 days, the crystals with the dimension of $8 \times 7 \times 1$, $19 \times 7 \times 1$ and $20 \times 6 \times 1$ mm³ from the saturated solution with 0.001 M concentration were harvested (Fig. 1).

3 Results and discussion

3.1 Phase structural analysis

Structural parameters of the grown pure and doped DAST crystals were analyzed by SXRD and PXRD patterns. SXRD result reveals that the grown pure and doped DAST crystals belongs to monoclinic structure and the corresponding lattice parameters were more agreement with the reported literature, which are tabulated in Table 1. PXRD patterns of the grown crystals were analyzed by Rich Seifert X-ray powder diffractometer with CuK α radiation ($\lambda = 1.5408$ Å) between the scattering angle of 10°–50° (Fig. 2). The well defined diffraction peaks authenticated the crystalline nature of grown DAST crystals.

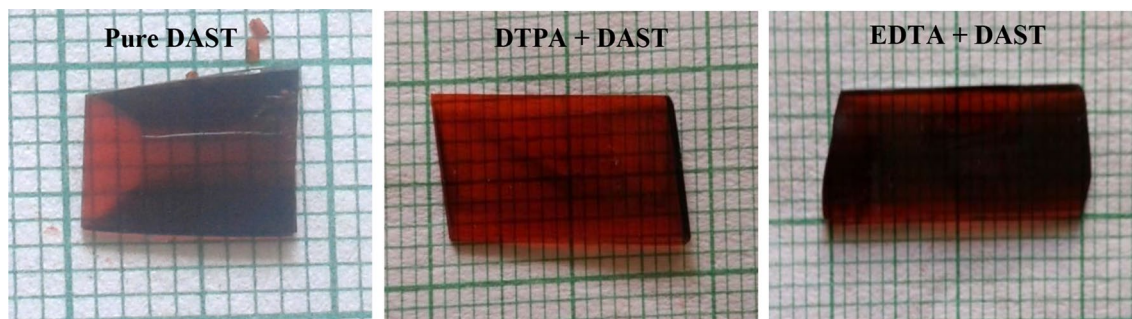
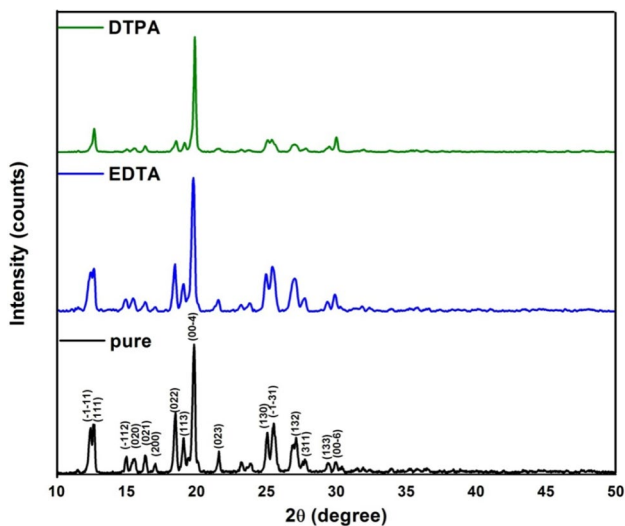


Fig. 1 Photograph of pure, DTPA and EDTA added DAST single crystals

Table 1 Lattice parameters of pure, EDTA and DTPA-doped DAST single crystals

Crystals	Lattice parameters (Å)					
	<i>a</i>		<i>b</i>		<i>c</i>	
	SXRD	PXRD	SXRD	PXRD	SXRD	PXRD
Pure DAST [21]	10.365 (3)	–	11.322 (4)	–	17.893 (4)	–
Pure DAST	10.341 (12)	10.212	11.301 (13)	10.617	17.845 (20)	18.061
EDTA + DAST	10.397 (12)	10.337	11.319 (12)	11.408	17.893 (20)	17.957
DTPA + DAST	10.366 (13)	10.397	11.232 (12)	11.421	17.892 (12)	17.867

**Fig. 2** Powder XRD pattern of pure, EDTA and DTPA-doped DAST crystals

However, the diffraction peak intensity of EDTA and DTPA-doped DAST crystals were slightly decreased due to the accumulation of additives in the crystalline structure, and a slight broadening was noticed in the of EDTA-doped DAST crystal which may be due to the presence of point defects and their aggregation. Such defects are common in all type of crystals including natural crystals which are unpreventable due to thermo dynamical conditions [4, 22]. Further, it is in clear vicinity that there are no additional peaks found in the X-ray diffraction pattern of EDTA and DTPA crystals, confirms that the structure of the DAST is not affected by the additives. The preferred orientation reflection peaks of pure and additives added DAST crystals are (111), (–112), (020), (021), (022), (004), (023), (130), (–1-31), (132), (311), (133), and (00–6) respectively, which are in close resemblance with the literature reports [16, 23].

3.2 UV-Vis spectral analysis

To find out the transmission limit and to probe the suitability of the grown single crystals of DAST towards optical applications, the optical transmission measurements was made

with Carry Varian 5000 spectrophotometer in the range of 200–800 nm at room temperature. The absorption spectra of pure, DTPA and EDTA added DAST crystals with the thickness of 0.70, 0.69, and 0.71 mm are shown in Fig. 3a. In comparison with pure DAST crystal, DTPA and EDTA added DAST crystals show significant red shifts and exhibit a less percentage of optical absorption after 550 nm. In addition, cut-off wavelength of pure and additives added DAST crystals are obtained at 524, 526 and 540 nm, respectively, in the visible region which demonstrate the suitability of these crystals for frequency doubling and optoelectronic applications [24]. The optical absorption coefficient (α) was determined with the following relation,

$$\alpha = \frac{2.303 \log \left(\frac{1}{T} \right)}{t}$$

where, t and T are the thickness of the sample and transmittance respectively. Moreover, band gap of the crystal is associated with the atomic and electronic structures and optical energy gap of the pure, EDTA and DTPA added DAST crystals has been obtained by applying the Tauc relation given as [25].

$$(\alpha h\nu)^{\frac{1}{n}} = A(h\nu - E_g)$$

where, ν is the photon's frequency, h is Planck's constant and A is the proportionality constant. Band gap of pure, DTPA and EDTA added DAST crystals are calculated by plotting $(\alpha h\nu)^{1/2}$ versus $h\nu$ as shown in Fig. 3b and extrapolating the linear portion near the onset absorption edge of the energy axis. The calculated band gap of grown crystals from Tauc plot were found to be 2.42, 2.46 and 2.35 eV for pure, DTPA and EDTA added DAST crystals respectively. This change in band gap is associated with various parameters including structural disorder, and lattice strain, wherein addition of dopants may enhance the density of localized states, thereby changing the band gap of the material [26]. The exhibited wide range of band gap energy values suggests the suitability of the grown crystals for optoelectronic applications [27].

The linear refractive index as a function of wavelength is crucial for developing NLO devices such as an electro-optic

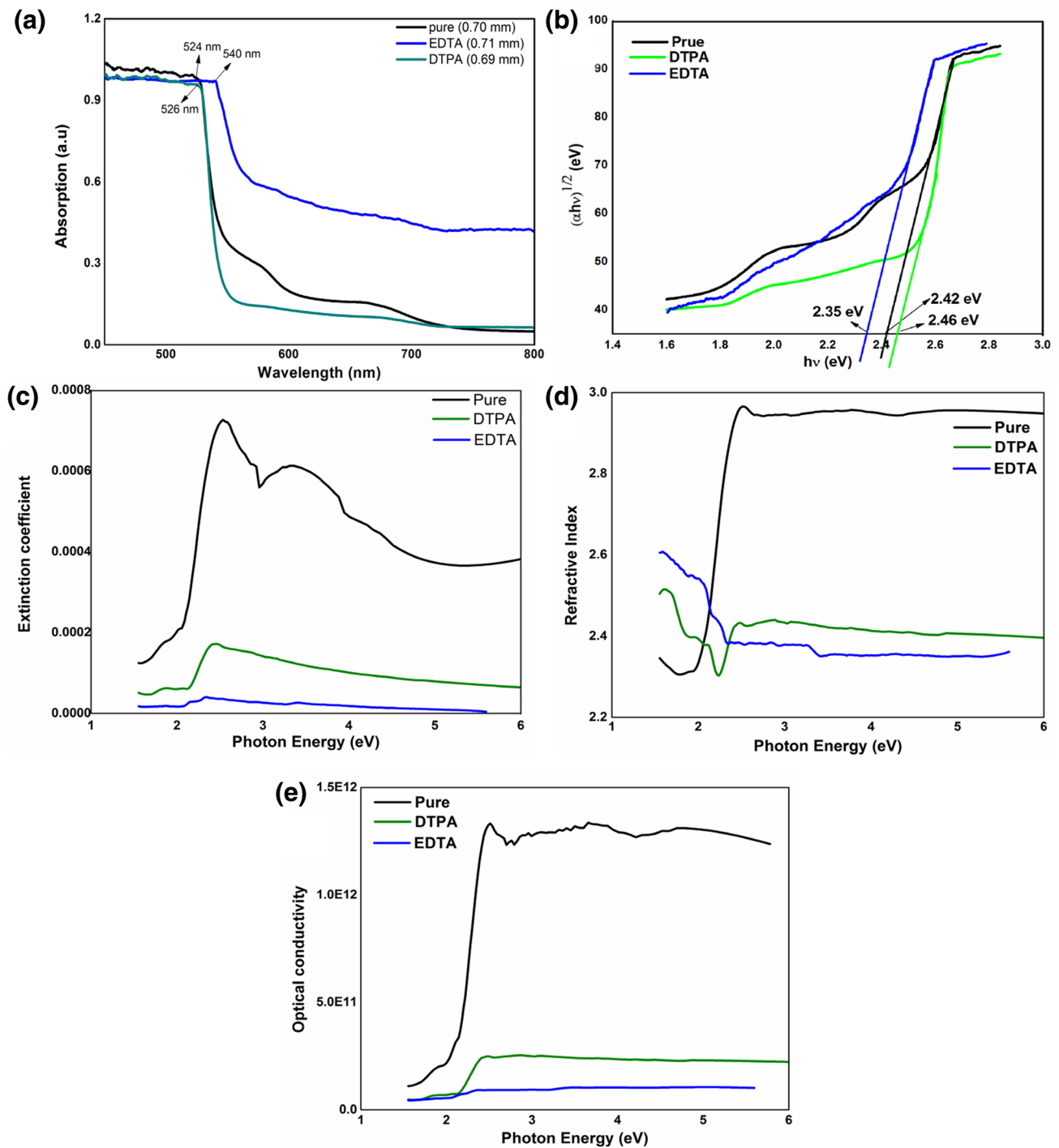


Fig. 3 **a** UV–Vis absorption spectra. **b** Plot of $(\alpha hv)^{1/2}$ versus $h\nu$. **c** Extinction coefficient. **d** Refractive index and **e** optical conductivity of pure and additives added DAST crystals

modulator, optical parametric oscillator and second harmonic generator. Large refractive index materials has lots of application in optoelectronic device fabrication such as advanced display systems, organic light emitting diodes

(OLEDs), anti-reflecting coating, power lenses, dispersive prisms and image sensors etc. [28]. The refractive index of a material is depends on wavelength of incident light, lattice mismatch, crystal composition, carrier density and

temperature [29]. Moreover, refractive index is vital to calculate the phase matching angles for NLO crystals [30]. The extinction coefficient (K) is obtained from the equation given as

$$K = \frac{\lambda\alpha}{4\pi}$$

where λ is the wavelength of the incident radiation. The obtained extinction coefficient of the pure, EDTA and DTPA-doped DAST crystals with respect to photon energy are shown in Fig. 3c. The reflectance of the crystal could be evaluated in terms of the absorption coefficient by applying the equation [31],

$$R = \frac{\exp(-\alpha t) \pm \sqrt{\exp(-\alpha t)T - \exp(-3\alpha t)t + \exp(-2\alpha t)T^2}}{\exp(-\alpha t) + \exp(-2\alpha t)T}$$

From the estimated reflectance value the refractive index of the material is evaluated using the expression [31],

$$n = \frac{-(R+1) \pm \sqrt{3R^2 + 10R - 3}}{2(R-1)}$$

Linear refractive indices (n) were calculated in terms of reflectance and the calculated linear refractive indices (Fig. 3d) of the pure, DTPA and EDTA added DAST crystals were found to be 2.43, 2.51 and 2.60 at the wavelength of 800 nm. The calculated refractive index of pure DAST crystal is found to be very close to the literature [21]. The resultant refractive index of additives doped DAST crystals shows higher values while comparing with pure DAST crystal due to the polarizability of the doped EDTA and DTPA atoms.

The optical conductivity is one of the significant tools to understand the electronic states in the materials. The optical conductivity (σ_{oc}) of a crystal mainly depends on the optical absorption coefficient through the following equation,

$$\sigma_{oc} = \frac{anC}{4\pi}$$

where C is the velocity of light. The optical conductivity against photon energy shows (Fig. 3e) an increasing trend with increase in photon energy and after the cut-off region it remains constant. However, the increase in optical conductivity is due to the amount of photons absorbed and the excitation of electrons by incident photon energy.

3.3 Laser damage threshold (LDT)

The crystals' stability against intense nanosecond/picosecond laser pulses is one of the most significant prerequisites for materials used in nonlinear and optoelectronics industry. As the frequency conversion efficiency of nonlinear optical single crystal is not only depends on the optical properties

of the crystal, but also on the intensity of incident laser [14]. A tiny scratch or even a small contagion on the surface of the crystal can largely reduce the surface damage threshold range [32]. The LDT of a material depends on the pulse width, wavelength of laser beam, thermal conductivity, thermal diffusivity, quality of crystal surface, laser intensity, density of effects, optical absorption and specific heat, etc. Hence, the thermal properties of the material play a vital role in LDT, which induces melting and decomposition due to the focus of high power laser. In particular, the thermal diffusivity of the crystal carries the surface temperature rapidly through the crystal from high temperature region to lower temperature region, which help the crystals to withstand large power and prevent the crystal from thermal damages [33].

In the present study, the samples used for LDT were cautiously chosen from the grown crystals with best quality and less defects. Plate-like well-polished crystals of pure, EDTA and DTPA added DAST crystals with 1 mm in thickness were subjected for the LDT analysis. A Q-switched Nd:YAG laser light of 1064 nm wavelength with the repetition rate of 10 Hz and pulse width 6 ns was focused on the (001) plane of the crystals using a convex lens with 15 cm focal length. The experiment was performed for pure; EDTA and DTPA added DAST crystals and the required energy to damage the crystal surface were measured as 69.2, 83.2 and 84.6 mJ. The laser damage threshold of the grown pure and additives added DAST crystal was calculated by applying the relation [34],

$$\text{Laser damage threshold} = \frac{E}{r^2 \tau \pi}$$

where, E is the applied input energy of laser (mJ), r is the radius of the circular laser spot size (mm), τ is the pulse width of the incident laser (ns).

Thus, the calculated laser damage threshold of grown pure, EDTA and DTPA-doped DAST crystals were found to be 2.71, 4.06 and 4.35 GW/cm², respectively. The observed

Table 2 Comparative analysis of LDT of DAST crystal with some benchmark crystals

Crystals	LDT values (GW/cm ⁻²)	References
BMP	4.16	[34]
KDP	0.20	[39]
BBO	5.0	[39]
Urea	1.5	[39]
L-tartaric acid	5.4	[40]
Pure DAST	2.8	[11]
Pure DAST	2.71	Present work
DAST + EDTA	4.06	Present work
DAST + DTPA	4.35	Present work

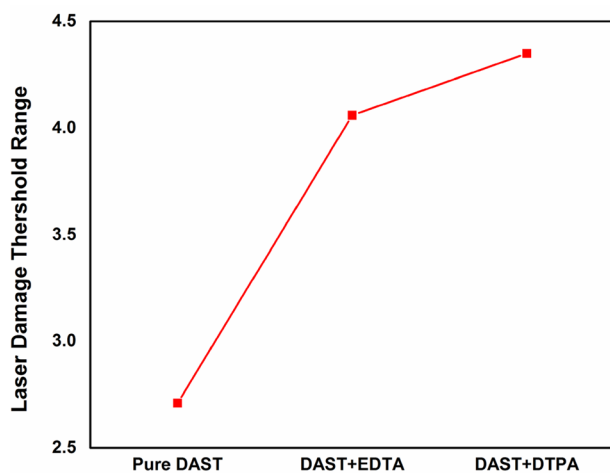


Fig. 4 Comparison of laser damage threshold of pure and additives added DAST crystal

LDT values of pure DAST crystals is in well agreement with the literature and it is compared with some well known benchmark organic and inorganic crystals (Table 2). The LDT values of EDTA and DTPA-doped DAST crystals are found to be 1.5 and 1.6 times higher (Fig. 4) than the pure DAST crystal, which shows better crystalline perfection, presence of less defects and higher mechanical stability [35–38].

3.4 Photoconductivity analysis of DAST crystal

Photoconductivity is a technique employed to understand the electrical and optical characteristics of materials when the electromagnetic radiation such as ultraviolet light, visible light or gamma radiations falls on the material's surface. The carrier density, complex process of carrier generation, recombination, and trapping are the basic phenomenon to understand the photoconductivity nature of a material [41]. The dark current and photocurrent measurement of the grown crystals were evaluated with the help of KEITHLEY 6487 picoammeter with the DC electric field at room temperature. Thin copper electrodes are fixed on the well-polished crystal's (001) surface using silver paste and sealed in vacuum chamber from all types of radiation and the applied input voltage was varied from 0 to 50 V (DC) in steps of 2 V and the corresponding dark current was measured. Then the experiment was repeated with light radiation using a 50 W halogen lamp and the resultant current was measured as photo current.

Figure 5a–c represents the change in photo current and dark current of the pure and doped DAST crystals at ambient temperature. It is noticed that the magnitude of dark current is larger than the photo current at all applied voltage for pure and EDTA-doped DAST crystals, which reveal the crystals exhibit negative photoconducting behavior which may be due to decrease in charge carriers and lifetime of photons during the light radiation [42, 43]. Since, the forbidden gap consisting of two energy levels, first one is among the conduction band and Fermi level, while the other one is near valence band. As the valence band has a more capture cross-section for holes and electrons, the valence band captures the charge carriers from the conduction band; consequently the flow of current is reduced in the presence of light radiation. Moreover, the DTPA added DAST crystal exhibits positive photoconductivity by conducting less dark current than the photo current, which may be attributed to the induced mobile charge carriers by the absorption of photons [44]. The photosensitivity of the pure and doped DAST crystals were calculated from the following relation,

$$S = \frac{\sigma_{ph}}{\sigma_{dr}}$$

where, σ_{ph} and σ_{dr} are the amount of photocurrent and dark current generated by the samples, respectively. Due to the presence of dopant atoms in the lattice level, the grown EDTA and DTPA-doped DAST crystals exhibit high photosensitivity (Table 3), which reveals the grown crystals are much suitable for optoelectronic applications [45].

3.5 Etching analysis

Device fabrication demands good quality of the crystals with fewer defects. Etching is one of the simple and most powerful techniques for understanding the growth features of crystal such as grain boundaries, solvent inclusions, dislocations, vacancy, cracks, stacking faults and microstructural imperfections, etc., which influence various physical properties such as mechanical strength and optical properties, etc. Thus, it is very essential to study the concentration of dislocations in the crystals [46, 47].

For this intention, the etching analysis was carried out for the grown pure, EDTA and DTPA-doped DAST crystals. The chemical etching was done by placing a drop of etchant (methanol) over the crystal surface for a time interval (5 s) and the etchant is wiped with soft tissue paper before it is examined by a transmission optical microscope at 100× magnification. The etch pattern of pure DAST crystal

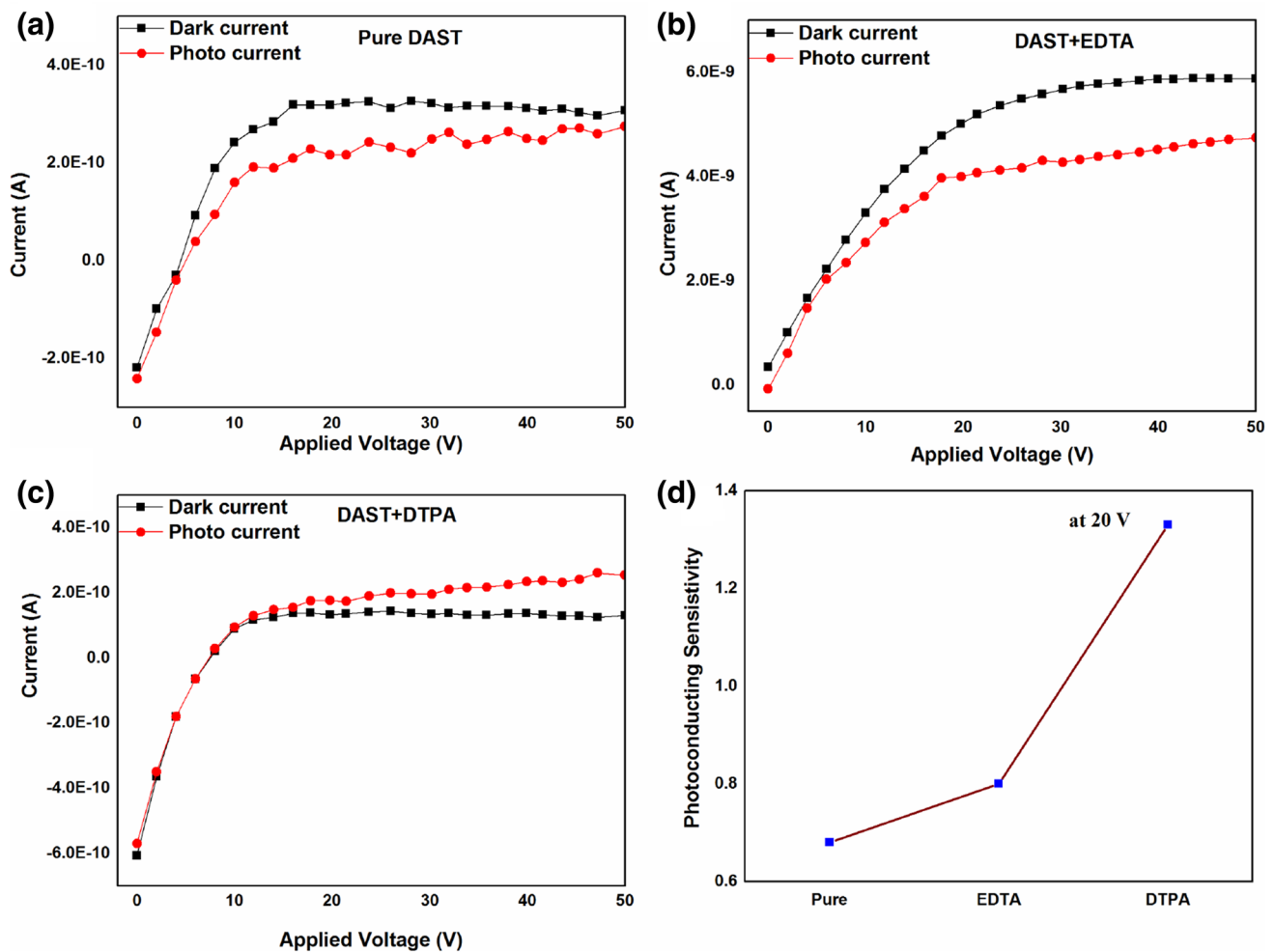


Fig. 5 a–d Photoconductivity and photosensitivity of pure and doped DAST single crystals

Table 3 Photosensitivity of pure and doped DAST single crystals

S. no.	Crystal	Photosensitivity (at 20 V)
1	DAST	0.68
2	EDTA + DAST	0.80
3	DTPA + DAST	1.33

(Fig. 6a) shows a number of spherical, oval, rectangular, and some irregularly shaped and misaligned etch pits, while the EDTA and DTPA-doped DAST crystals (Fig. 6b, c) show smooth and linear layered well defined etch pits. In addition, the doped crystals illustrate very few etch pits, which is associated with the systematic arrangement of atoms or molecules. This confirms the quality of EDTA and DTPA-doped DAST crystals are better than the pure DAST crystal.

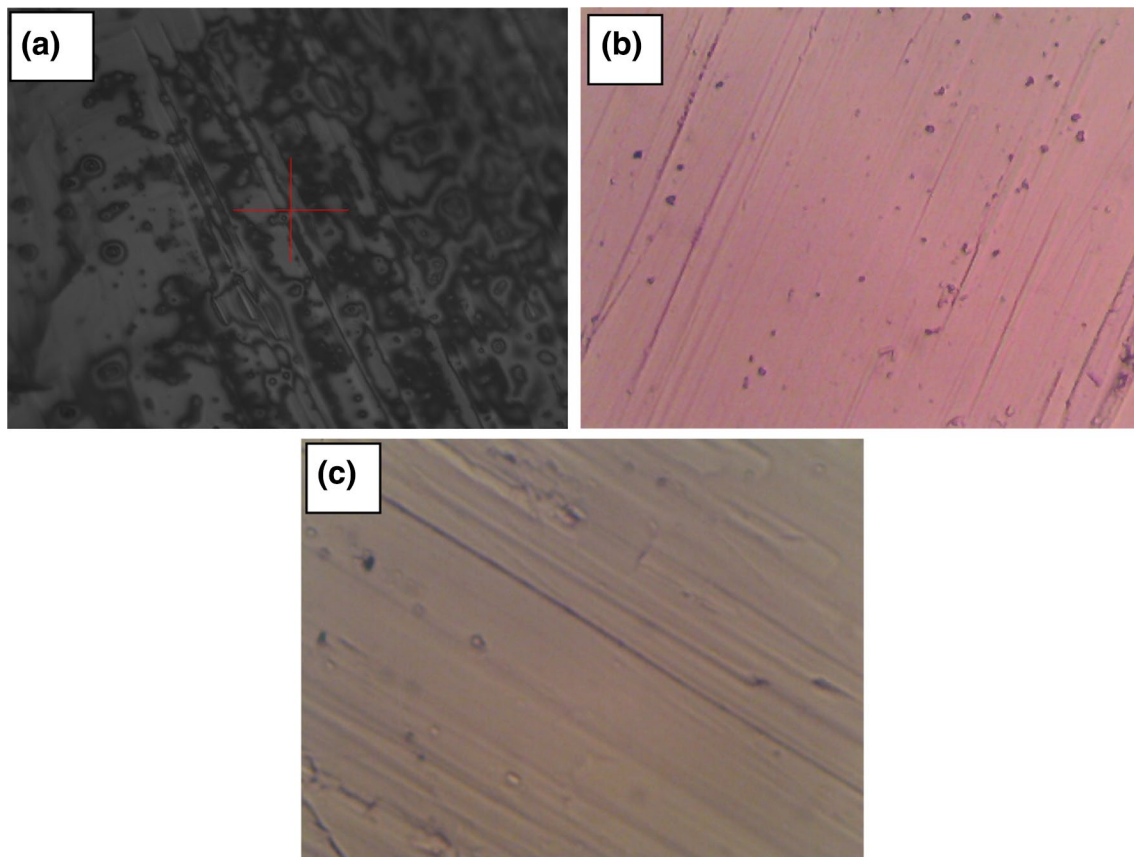


Fig. 6 Etch pit patterns of **a** pure **b** EDTA-doped DAST and **c** DTPA-doped DAST crystals

4 Conclusions

A relatively bulk size organic DAST single crystals were grown in the presence of EDTA and DTPA by controlled solvent evaporation method at ambient temperature. Single crystal and powder crystal X-ray diffraction analysis results evidenced that grown crystals are in monoclinic structure. The optical band gaps of pure, EDTA and DTPA-doped DAST crystals were found to be 2.42, 2.46 and 2.35 eV, respectively. Linear refractive indices of pure, DTPA- and EDTA-doped DAST crystals were found to be 2.43, 2.51 and 2.60 at 800 nm. DTPA added DAST crystal exhibits higher laser damage threshold than those of the other crystals. Photoconductivity study reveals that the pure and EDTA-doped DAST crystals possess negative photoconducting behaviour while DTPA-doped DAST crystal shows positive photoconducting behaviour. Enhanced crystalline perfection of EDTA and DTPA-doped DAST crystal is evident from the etch patterns.

Acknowledgements The authors (M. Manivannan, S. A. Martin Britto Dhas, and M. Jose) gratefully acknowledge the Department of Atomic Energy-Board of Research in Nuclear Sciences (DAE-BRNS),

Government of India for the financial support (Sanction Number: 34/14/54/2014-BRNS).

References

1. M. Rajkumar, A. Chandramohan, *Opt. Mater.* **66**, 261 (2017)
2. H. Redrothu, S. Kalainathan, G. Bhagavannarayana, *Optik* **124**(18), 3718 (2013)
3. A. Saranraj, S. Sahaya Jude Dhas, G. Vinita, S.A.M.B. Dhas, *Mater. Res. Express* **4**(10), 1 (2017)
4. M. Jose, B. Sridhar, G. Bhagavannarayana, K. Sugandhi, R. Uthrakumar, C. Justin Raj, D. Tamilvendhan, S.J. Das, *J. Cryst. Growth* **312**, 793 (2010)
5. S. Vanishri, H.L. Bhat, A. Deepthy, V.P. Nampoore, E. de Matos Gomes, *J. Appl. Phys.* **99**, 083107 (2006)
6. L. Mutter, P. Dittrich, M. Jazbinsek, P. Gunter, *J. Nonlinear Opt. Phys. Mater.* **13**(3 & 4), 559 (2004)
7. J. Ramajothi, S. Dhanuskodi, K. Nagarajan, *Cryst. Res. Technol.* **39**(5), 414 (2004)
8. X. Liu, Z. Yang, D. Wang, H. Cao, *Crystals*, **158**(6), 1 (2016)
9. P.J. Hale, J. Madeo, C. Chin, S.S. Dhillon, J. Mangeney, J. Tignon, K.M. Dani, *Opt. Express* **22**(21), 26358 (2014)
10. S. Brahadeeswaran, Y. Takahashi, M. Yoshimura, M. Tani, S. Okada, S. Nashima, Y. Mori, M. Hangyo, H. Ito, T. Sasaki, *Cryst. Growth Des.* **13**, 415 (2013)

11. Y. Takahashi, S. Onduka, S. Brahadeeswaran, M. Yoshimura, Y. Mori, T. Sasaki, *Opt. Mater.* **30**, 116 (2007)
12. Z. Sun, T. Chen, J. Luo, M. Hong, *J. Cryst. Growth* **328**, 89 (2011)
13. S. Zhuang, B. Teng, L. Cao, D. Zhong, K. Feng, Y. Shi, Y. Li, Q. Guo, M. Yang, *Adv. Mater. Res.* **709**, 36 (2013)
14. B. Babu, J. Chandrasekaran, B. Mohanbabu, Y. Matsushita, M. Saravanakumar, *RSC Adv.* **6**, 110884 (2016)
15. S.-J. Kwon, M. Jazbinsek, O.-P. Kwon, P. Gunter, *Cryst. Growth Des.* **10**(4), 1552 (2010)
16. A.S. Haja Hameed, S. Rohani, W.C. Yu, C.Y. Tai, C.W. Lan, *Mater. Chem. Phys.* **102**, 60 (2007)
17. B. Liu, Y. Yang, Y. Zhang, X. Lv, L. Wei, X. Wang, *J. Mater. Sci. Mater. Electron.* **26**(10), 8097 (2015)
18. P. Rajesh, A. Silambarasan, P. Ramasamy, *Mater. Res. Bul.* **49**, 640 (2014)
19. T. Ananthi, S. Mary Delphine, M. Mary Freeda, R. Krishna Priya, A.W. Almusallam, *Rec. Res. Sci. Technol.* **3**, 32 (2011)
20. M. Manivannan, S.A.M.B. Dhas, M. Jose, *J. Cryst. Growth* **455**, 161 (2016)
21. S.R. Marder, J.W. Perry, C.P. Yakymyshyn, *Chem. Mater.* **6**, 1137 (1994)
22. S. Supriya, S. Kalainathan, G. Bhagavannarayana, *J. Phys. Chem. Solids* **74**, 70 (2013)
23. M. Manivannan, S.A.M.B. Dhas, M. Jose, *J Inorg Organomet Polym* **27**, 1870 (2017)
24. N. Vijayan, R. Ramesh Babua, R. Gopalakrishnan, P. Ramasamy, M. Ichimura, M. Palanichamy, *J. Cryst. Growth* **273**, 564 (2005)
25. J. Tauc, R. Grigorovici, A. Vanc, *Phys. State Sol.* **15**, 627 (1966)
26. E. Yucela, Y. Yucel *Opticals* **142**, 82 (2017)
27. B.K. Periyasamy, S. Robinson, Jebas, B. Thailampillai, *Mater. Lett.* **61**, 1489 (2007)
28. J. Liu, M. Ueda, *J. Mater. Chem.* **19**, 8907 (2009)
29. B. Broberg, S. Lindgren, *J. Appl. Phys.* **55**, 3376 (1984)
30. F. Koohyar, *J. Thermodyn. Catal.* **4:2**, 1000e117 (2013)
31. K. Thukra, N. Vijayan, B. Rathi, G. Bhagavannarayana, S. Verma, J. Philip, A. Krishna, M.S. Jeyalakshmy, S.K. Halder, *Cryst. Eng. Commun.* **16**, 2802 (2014)
32. A. Silambarasan, P. Rajesh, R. Bhatt, I. Bhaumik, A.K. Karnal, P. Ramasamy, P.K. Gupta, *Appl. Phys. A* **122:736**, 1 (2016)
33. V. Sivasubramani, V. Mohankumar, M. Senthil Pandian, P. Ramasamy, S.A.M.B. Dhas *J. Mater. Sci. Mater. Electron.* **29**(3), 2091 (2018)
34. K. Arunkumar, S. Kalainathan, *Opt. Laser Technol.* **89**, 143 (2017)
35. M. Senthil Pandian, P. Ramasamy, *Mater. Chem. Phys.* **132**, 1019 (2012)
36. D.J. Daniel, P. Ramasamy, *Opt. Mater.* **36**, 971 (2014)
37. M. Senthil Pandian, P. Ramasamy, *J. Cryst. Growth* **312**, 413 (2010)
38. P. Rajesh, P. Ramasamy, G. Bhagavannarayana, B. Kumar, *Curr. Appl. Phys.* **10**, 1221 (2010)
39. N. Vijayan, G. Bhagavannarayana, R. Ramesh Babu, R. Gopalakrishnan, K.K. Maurya, P. Ramasamy, *Cryst. Growth Des.* **6**(6), 1542 (2006)
40. S.A.M.B. Dhas, G. Bhagavannarayana, S. Natarajan, *J. Cryst. Growth* **309**, 48 (2007)
41. R. Shankar, R.K. Srivastava, *Proc. Natl. Acad. Sci. India Sect. A Phys. Sci.* **88**, 1 (2017)
42. R. Jerald Vijay, N. Melikechi, T.R. Kumar, G.M. Joe, P.J. Sagaraj, *J. Cryst. Growth* **312**, 420 (2010)
43. C. Justin Raj, S. Dinakaran, S. Krishnan, B. Milton Boaz, R. Robert, S.J. Das, *Opt. Commun.* **281**, 2285 (2008)
44. S. Chandran, R. Paulraj, P. Ramasamy, *Opt. Mater.* **52**, 49 (2016)
45. Y.L. Chu, X.H. Wu, J.J. Lu, D.P. Liu, J. Du, G.Q. Zhang, P.J. Huang, *Adv. Sci.* **3**, 1500435 1 (2016)
46. S.P. Ramteke, M.I. Baig, M. Shkir, S. Kalainathan, M.D. Shirsat, G.G. Muley, M. Anis, *Opt. Laser Technol.* **104**, 83 (2018)
47. V. Ganesh, C.S. Reddy, M. Shkir, M.A. Wahab, G. Bhagavannarayana, K. Kishan Rao, *Physica B* **406**, 259 (2011)